[28] S. Mann and S. Haykin, "The chirplet transform—Physical considerations," *IEEE Trans. Signal Process.*, vol. 43, no. 11, pp. 2745–2761, Nov. 1995.
[29] S. G. Mallat and Z. Zhang, "Matching pursuit with time-frequency dictionaries," *IEEE Trans. Signal Process.*, vol. 41, no. 12, pp. 3397–3415, Dec. 1993.

# The Influence of CSF on EEG Sensitivity Distributions of Multilayered Head Models

K. Wendel, *Student Member, IEEE*, N. G. Narra, M. Hannula, P. Kauppinen, and J. Malmivuo, *Fellow, IEEE*

***Abstract*—We examined how the cerebrospinal fluid (CSF) affects the distribution of electroencephalogram (EEG) measurement sensitivity. We used concentric spheres and realistic head models to investigate the difference between computed-tomography (CT) and magnetic resonance image (MRI) models that exclude the CSF layer. The cortical EEG sensitivity distributions support these phenomena and show that the CSF layer significantly influences them, thus identifying the importance of including the CSF layer inside the head volume conductor models. The results show that the highly conductive CSF channels the current, thus decreasing the maximum cortical current density relative to models that do not include the CSF. We found that the MRI and CT models yielded HSV results 20% and 45%, respectively, too small when compared with CSF-inclusive models.**

***Index Terms*—Conductivity, cerebrospinal fluid (CSF), electroencephalogram (EEG), lead field current density, sensitivity distribution, volume conductor.**

## I. Introduction

Traditionally head models have been constructed as three concentric spheres [1]–[3], modeling the scalp, skull, and brain. Recently, realistic models are constructed from a set of segmented image slices, usually originating from one of the primary medical imaging modalities—computed tomography (CT) or magnetic resonance images (MRI). Considering their pros and cons, CT more accurately images the skull due to its sensitivity to hard tissue, whereas MRI better images soft tissues such as the skin, cortex, and the gray matter-white matter boundary [4]. The differences between the three-layer CT- and MRI-based models in [4] illustrate significant differences at the base of the skull.

The cerebrospinal fluid (CSF) layer, which surrounds the brain, is often neglected either due to the difficulty to correctly segment this layer from T1- and T2-weighted MRIs [5] or the insensitivity of CT images to soft tissues. The omission of the CSF layer can alter the segmentation via incorporation into the skull or into the brain (gray matter). Some realistic head models explicitly define the skull as the region between the scalp and the cortex, whereas, other models define the brain as the region inside the skull [4]. MRI-based models by Ramon *et al.* [5] include the CSF layer and indicate the significance this layer has on scalp potentials and on the inverse source localizations.

By incorporating CSF in one type of head model and removing it from the other two, we examine the role of CSF and how it affects the images of the two modalities that do not directly include this layer. We use both spherical and realistic models to investigate the sensitivity distributions. In this work, we construct head models representing a matched MRI-CT- (i.e., CSF inclusive), MRI-, and a CT-based model. These models identify the significance of including the CSF layer inside the head volume conductor model by studying how electrode separation affects the cortical sensitivity distributions.

Manuscript received March 12, 2007; revised September 4, 2007. This work was supported by the Finnish Funding Agency for Technology and Innovation (TEKES), the Ragnar Granit Foundation, and the International Graduate School of Biomedical Engineering and Medical Physics, Finland. *Asterisk indicates corresponding author.*

*K. Wendel is with the Ragnar Granit Institute, Department of Electrical Engineering, Tampere University of Technology, 33101 Tampere, Finland (e-mail: katrina.wendel@tut.fi).

N. G. Narra, M. Hannula, P. Kauppinen, and J. Malmivuo are with the Ragnar Granit Institute, Department of Electrical Engineering, Tampere University of Technology, 33101 Tampere, Finland.

Digital Object Identifier 10.1109/TBME.2007.912427

## II. Methods

### A. Model Geometries

We used spherical models to illustrate the general results and to reveal the underlying phenomena. We modeled four concentric spheres with radii of 7.45, 7.80, 8.45, and 9.0 cm for the brain, CSF, skull, and scalp, respectively [6]–[8]. We use realistic models to validate the spherical model findings. We segmented the Visible Human Woman (VHW) from the Visible Human Project [9] since tissue segmentation eliminates the MRI-CT data set registration. These models are constructed by addressing the tissues separately. Each tissue was segmented, slice contoured, and lofted together

In both the spherical and realistic sets, the three-layer CT-model defines the brain as the region inside the interior skull boundary; the three-layer MRI-model defines the skull as the region between the skull exterior and the brain exterior; the four layer CSF-model defines the CSF as the layer between the skull interior and the brain exterior. A fourth set, the three-layer CT2 model, is based on the CT-model results but excludes the cortical results that lie outside the actual brain exterior (i.e., the CSF). Finally, we calculate the CT2 sensitivity volumes and maximum current density values from only the volume contained by the actual brain.

We spaced all electrodes between $10^\circ$ and $40^\circ$ apart. Furthermore, we calculated that the smallest adjacent bipolar lead pair of the 256-, 128-, 64-, and 32- channel electroencephalogram (EEG) electrode montages is represented by spherical angles $11^\circ$, $18^\circ$, $23^\circ$, and $31^\circ$, respectively. We fitted our spherical angles according to standard EEG nomenclature [10]. We modeled all electrodes as 3-D simple recessed electrodes [11] with radii of 5 mm, corresponding to the size of high-resolution EEG caps [3]. Since the analytical model solves for the point electrode [12], we constructed finite-element method models and meshed them with tetrahedral adaptive meshes via COMSOL Multiphysics, COMSOL Group, Sweden.

### B. Sensitivity Distribution Simulations

We simulated the sensitivity distributions through a range of tissue conductivities. We modeled the brain, CSF, and scalp compartments as 0.25, 1.79, and 0.45 S/m, respectively [13], [7]. The skull was modeled using brain-to-skull conductivity ratios $\sigma_{Br}/\sigma_{Sk}$ of 5, 10, 15, 20, and 80 according to [14]. The sensitivity distributions are calculated according to the current density $\mathbf{J}$, where

$$\mathbf{J} = -\sigma \nabla \Phi + \mathbf{J}^e \tag{1}$$

is a function of the scalar potential $\Phi$ and the externally applied current density $\mathbf{J}^e$, assuming bioelectric currents and voltages to be quasi static [6]. We fed a $1A$ reciprocal current into a source electrode flowing to a grounded electrode. The distribution of the current in the model maps the lead field, i.e., the measurement sensitivity distributions. We

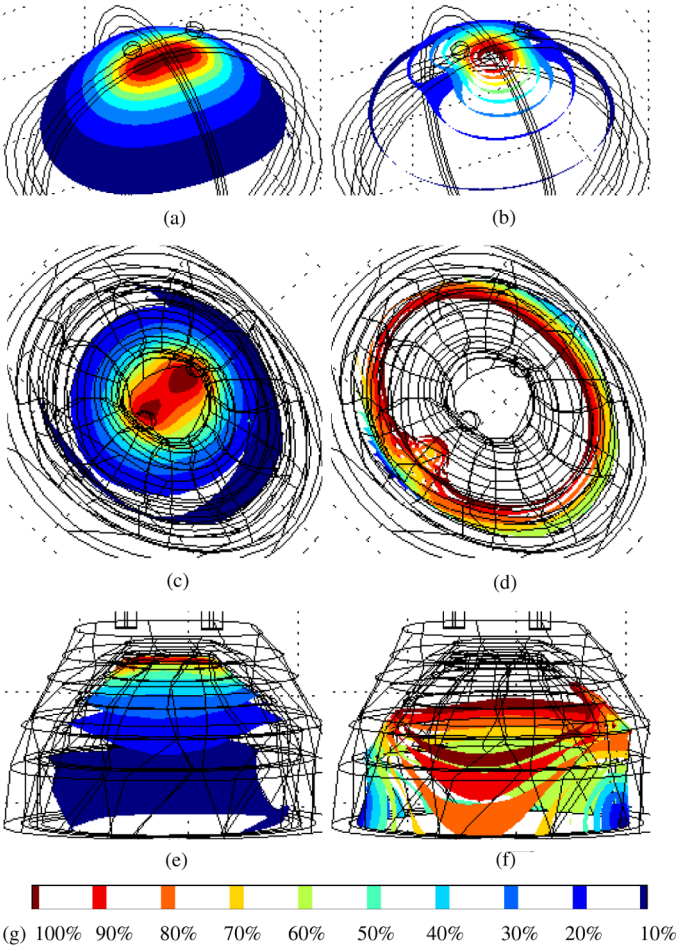


Fig. 1. Three-dimensional isosensitivity distributions. (a)–(f) All subfigures evaluate the CSF model with electrodes spaced 25° and $\sigma_{Br}/\sigma_{Sk} = 10$. The electrodes are the two small cylindrical disks in each figure. All subcaptions list the type of isosensitivity distribution and the camera angle. (a) and (b) map the spherical version and (c)–(f) map the realistic model. (a), (c), and (e) depict the brain isosensitivity distributions. (b), (d), and (f) depict the CSF isosensitivity distributions. (g) The isosurface colorbar designates ten increments diminishing from 100% to 10% current density values for each subfigure. The top 50% indicates the HSV, and the top 20% indicates the FSV. (a) Brain: Top View. (b) CSF: Top View. (c) Brain: Top View. (d) CSF: Top View. (e) Brain: Side View. (f) CSF: Side View. (g) 100%, 90%, 80%, 70%, 60%, 50%, 40%, 30%, 20%, and 10%.

analyzed the simulations by comparing the half sensitivity volumes (HSVs) [2] and introduce the fifth sensitivity volume (FSV) to outline the area of the top 50% and 20%, respectively, of the current density isosensitivity surfaces within the brain.

## III. Results

Over 90% of the whole head reciprocal current density resides in the scalp for electrode pairs closer than 60°. Between 1% and 2% of the head lead field current distribution enters the cortical regions of only the CSF-spherical models, while less than 1% of the distribution enters the cortical regions for the CT- and MRI-spherical models. Fig. 1 illustrates the HSV and FSV of the 3-D brain and CSF lead field isosensitivity distributions for a CSF head model representing a 64-channel bipolar lead configuration. Fig. 1(a), (b), and (c)–(f) depicts the spherical and realistic solutions, respectively.

Fig. 2 graphs the quantitative results of the models with $\sigma_{Br}/\sigma_{Sk}$ of 10 and 80. The graphs in the top row and bottom row represent the spherical and realistic results, respectively. The left column of graphs plots the maximum-cortical current density versus electrode separation angle. The middle and right columns chart the HSV and FSV results, respectively. The difference between the recently revised $\sigma_{Br}/\sigma_{Sk}$ of 10 and the historical ratio of 80 ranges from 50% to 110% larger for electrode angles ranging from 10° to 40°, respectively, for the CSF-model HSV results.

The MRI model nearly matches the CSF profile in the normalized lead field sensitivity distributions [Fig. 2(b), (e), and (f)]. The HSV of the MRI model is approximately 20% to 25% smaller than the CSF model for $\sigma_{Br}/\sigma_{Sk}$ of 10. However, the maximum reported MRI current density values show that the combination of the thicker skull and the exclusion of the highly conductive CSF layer yield relatively higher current density values than the CSF models (Fig. 2). When we compare the results of the MRI model with the historical $\sigma_{Br}/\sigma_{Sk}$ of 80 with the contemporary CSF model, the HSV of the MRI model is within $\pm 5\%$ of the CSF model.

The CT model provides the highest lead field cortical current density and the finest spatial resolution [i.e., the smallest sensitivity volumes; see Fig. 2(b), (c), (e), and (f)]. Although the CT model has the same skull thickness as the CSF model, more current enters the cortical region of the CT model than the CSF model by 350% to 400%. The HSV of the CT model resolves approximately 45% to 50% smaller than the CSF model, whereas the historical CT model results resolve 35% to 40% smaller than the contemporary CSF model.

## IV. Discussion

The current-diffusing nature of the thicker skull of the MRI model lacks the highly conductive CSF layer that concentrates the current within itself. However, the MRI model more closely identifies with the CSF brain pattern because MRI better images soft tissues. The result is a brain size consistent with the CSF model. Effectively, the current that does pass through the skull preferentially spreads in the higher conducting CSF layer and concentrates between the electrodes before entering the less conductive brain [Fig. 1(b) and (d)]. The CT model suffers from the combination of the skull not being thick enough to thwart more of the current flow and the lack of a highly conductive CSF layer to concentrate the current within the CSF. By converting the CT model to the CT2 model, it nearly mimics the CSF-model profile but still yields smaller FSVs and HSVs than the CSF model [Fig. 2(b) and (c)].

In general, the CT-model's sensitivity distributions differ mostly from the CSF model due to the fact that the brain region is enlarged. This difference dramatically changes the brain's lead field sensitivity distributions the farther the electrodes are separated. By compensating the CT2 model with the actual brain size, CT2 more closely represents the CSF model than the CT model. However, the shift in size does not incorporate the phenomena of the highly conductive CSF layer drawing the lead field sensitivity volume percentages slightly deeper into the whole head and brain.

## V. Conclusion

The relatively high conducting CSF layer attracts and concentrates the lead field current, thus partially shunting the current flow to the brain. Sensitivity distributions are also directly affected by the determination of the tissue boundaries according to an imaging modality. Since the CT model has a relatively thinner skull than the MRI model, more current passes through it to the brain. The thicker-than-realistic skulls of the MRI model performed spatially closer to the CSF model than the CSF-lacking CT model, although both map the HSVs and FSVs with smaller volumes than the equivalent CSF model. Therefore, head models should include the CSF layer due to its influence upon the cortical sensitivity distribution directly beneath the CSF layer. Consequently, EEG models that exclude the CSF layer will model the spatial

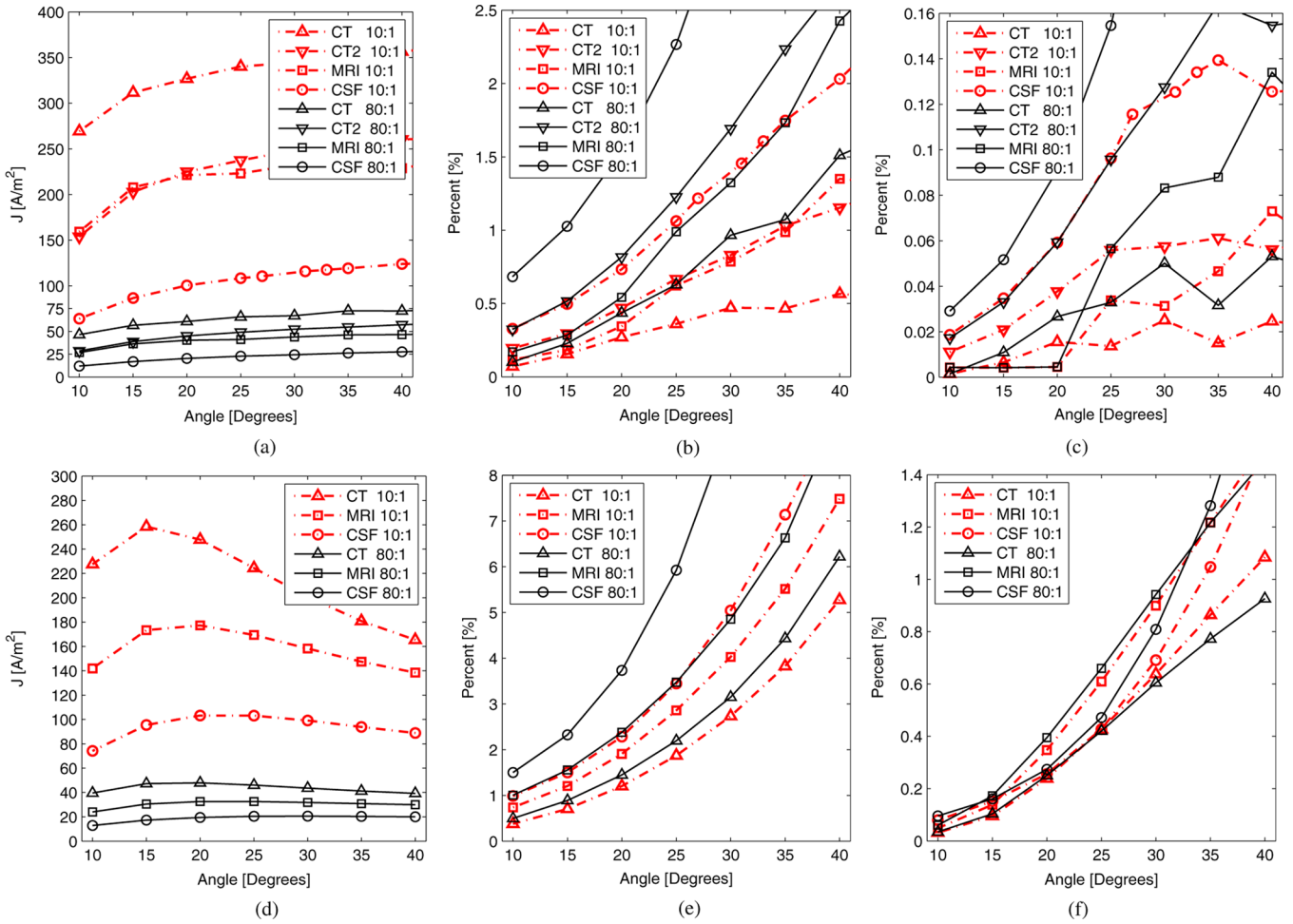


Fig. 2. (Top row) Spherical model results. (Bottom row) Realistic model results. (a), (d) Maximum cortical current density $\mathbf{J}\,[A/m^2]$ versus electrode separation angle. (b), (c), (e), (f) Percentage of the brain filled by (b), (e) the HSV and (c), (f) the FSV versus electrode separation angle. Angles 11°, 18°, 23°, and 31° approximate 256, 128, 64, and 32 EEG electrode montages, respectively [10]. (a) Current Density: $\sigma_{Br}/\sigma_{Sk} = 10$ and $80$, (b) HSV Percentage: $\sigma_{Br}/\sigma_{Sk} = 10$ and $80$, (c) FSV Percentage: $\sigma_{Br}/\sigma_{Sk} = 10$ and $80$, (d) Current Density: $\sigma_{Br}/\sigma_{Sk} = 10$ and $80$, (e) HSV Percentage: $\sigma_{Br}/\sigma_{Sk} = 10$ and $80$, (f) FSV Percentage: $\sigma_{Br}/\sigma_{Sk} = 10$ and $80$.

resolution better than it really is by approximately 20% and 45%, for MRI- and CT-based models respectively.

## REFERENCES


[1] S. Rush and D. Driscoll, "EEG electrode sensitivity—An application of reciprocity," *IEEE Trans. Biomed. Eng.*, vol. 16, no. 1, pt. , pp. 15–22, Jan. 1969.

[2] J. Malmivuo, V. Suihko, and H. Eskola, "Sensitivity distributions of EEG and MEG measurements," *IEEE Trans. Biomed. Eng.*, vol. 44, no. 3, pp. 196–208, Mar. 1997.

[3] J. Ollikainen, M. Vauhkonen, P. Karjalainen, and J. Kaipio, "Effects of electrode properties on EEG measurements and a related inverse problem," *Med. Eng. Phys.*, vol. 22, pp. 535–545, 2000.

[4] G. Huiskamp, M. Vroeijenstijn, R. van Dijk, G. Wieneke, and A. van Huffelen, "The need for correct realistic geometry in the inverse EEG problem," *IEEE Trans. Biomed. Eng.*, vol. 46, no. 11, pp. 1281–1287, Nov. 1999.

[5] C. Ramon, P. Schimpf, and J. Haueisen, "Influence of head models on EEG simulations and inverse source localizations," *BioMed. Eng. Online*, Feb. 2006.

[6] J. Malmivuo and R. Plonsey, *Bioelectromagnetism—Principles and Applications of Bioelectric and Biomagnetic Fields*. New York: Oxford Univ. Press, 1995.

[7] T. Ferree, K. Eriksen, and D. Tucker, "Regional head tissue conductivity estimation for improved EEG analysis," *IEEE Trans. Biomed. Eng.*, vol. 47, no. 12, pp. 1584–1592, Dec. 2000.

[8] T. Oostendorp, J. Delbeke, and D. Stegeman, "The conductivity of the human skull: Results of in vivo and in vitro measurements," *IEEE Trans. Biomed. Eng.*, vol. 47, no. 11, pp. 1487–1492, Nov. 2000.

[9] National Institutes of Health, U.S. National Library of Medicine, Visible Human Project [Online]. Available: http://www.nlm.nih.gov/research/visible/visible_human.html

[10] R. Oostenveld and P. Praamstra, "The five percent electrode system for high-resolution EEG and ERP measurements," *J. Clin. Neurophysiol.*, vol. 112, pp. 713–719, 2001.

[11] M. Suesserman, F. Spelman, and J. Rubinstein, "In vitro measurement and characterization of current density profiles produced by nonrecesed, simple recessed, and radially varying recessed stimulating electrodes," *IEEE Trans. Biomed. Eng.*, vol. 38, no. 5, pp. 401–408, May 1991.

[12] R. Gordon, T. Arola, K. Wendel, O. Ryynanen, and J. Hyttinen, M. Min, Ed., "Accuracy of numerical methods in solving static and quasistatic electric fields," in *Proc. the Estonian Acad. Sciences; Engineering*, Tallinn, Estonia, Sep. 2006, vol. 12/3-2, pp. 262–283.

[13] S. Baumann, D. Wozny, S. Kelly, and F. Meno, "The electrical conductivity of human cerebrospinal fluid at body temperature," *IEEE Trans. Biomed. Eng.*, vol. 44, no. 3, pp. 220–223, Mar. 1997.

[14] K. Wendel and J. Malmivuo, "Correlation between live and post mortem skull conductivity measurements," in *28th Ann. Int. Conf. IEEE Eng. Medicine and Biology Soc.*, Aug. 2006.